33rd Annual International Conference of the IEEE EMBS
Boston, Massachusetts USA, August 30 - September 3, 2011

Effect of Deep Breathing on Extracted Oxygen and Cerebral Hemoglobin Levels

Patrick M. Kennedy, Christopher M. Zarbock, Broc A. Burke,
and Solomon G. Diamond, *Member, IEEE*

***Abstract*— This study examines the relationship between oxygen expired and functional near infrared spectroscopy (fNIRS) measured hemoglobin levels in the brain. Analysis of these two signals during normal versus deep breathing provides insight into the dynamics of cerebral physiology. Intersubject variation suggests the existence of two distinct groups with respect to oxygen extraction and hemoglobin levels.**

I. Introduction

A. Respiration and Ventilation

Two separate muscle groups can independently induce pulmonary ventilation. Normal breathing is typically executed by concerted movements of the diaphragm and abdominal muscles. A second method is raising the rib cage, accomplished by the intercostal muscles. Typical breathing moves a tidal volume, or normal breath volume, of air. Deep breathing taps into the inspiratory and expiratory reserve volumes. These breathing methods likely have different physiological effects on the interface between the blood-gas composition of the body and the surrounding environment. Since deep breathing is a common therapy technique for a variety of diseases and conditions, including ADHD, anxiety, and insomnia, the motivation of this experiment was to understand the effects of deep breathing on a physiological level [1].

The source of blood-gas composition control is in the alveoli, where alveolar ventilation and alveolar blood flow are dynamically controlled. The change in alveolar ventilation over time is often described as

$$\frac{dV_{alveolar}}{dt} = \dot{V} = f_{resp}\left(V_{tidal} - V_{dead}\right), \quad (1)$$

where f_{resp} is the frequency of the respiration cycle and V_{tidal} is the volume of air displaced between normal inspiration and expiration. The dead volume can be found with the Bohr equation

$$\frac{V_{dead}}{V_{tidal}} = \frac{Pa_{CO_2,arterial} - Pe_{CO_2}}{Pa_{CO_2,arterial}}, \quad (2)$$

which relates V_{dead} to V_{tidal} through the partial pressure of CO_2 in the blood (Pa_{CO2}) and the expired partial pressure of CO_2 (Pe_{CO2}). The flow of gas in the blood, Q_{gas}, equals the product of the flow of blood, Q_{blood}, and the concentration of CO_2 in the veins and arteries (c_{venous} and $c_{arterial}$, respectively) by [2]

$$Q_{gas} = Q_{blood}(c_{venous} - c_{arterial}). \quad (3)$$

The relationship between $\dot{V}$ and Q_{gas} is known as the ventilation-perfusion rate. During periods of normal breathing, $\dot{V}/Q_{gas}$ rests at a steady state value. During periods of deep breathing, however, both the displaced volume and dead volume increase, increasing the ventilation-perfusion ratio to a higher steady state level [3].

B. Near Infrared Spectroscopy

Near Infrared Spectroscopy (NIRS) is a non-invasive technique used to measure functional hemoglobin concentration changes in the brain by utilizing the different absorbance spectra of oxy- and deoxyhemoglobin (HbO and HbR respectively) within the cerebral capillaries. The spatial sensitivity of NIRS is limited to the outer 1 cm of brain tissue due to the exponential loss of optical power with distance due to absorption. Three distinct NIRS methods exist, including: continuous wave (CW), frequency domain, and time domain systems. The CW technique is used for this experiment for its high temporal resolution, excellent signal to noise ratio, and relatively low cost for an array of sources and detectors [4].

C. Hypocapnia

It is well understood that with a higher ventilation rate, carbon dioxide is eliminated from the blood more efficiently. For the brain, this can lead to cerebral vasoconstriction and reduced cerebral blood flow (CBF) as a result of lower blood acidity due to the buffering of carbon dioxide with the bicarbonate ion [3]. This condition, known as hypocapnia, is defined as a reduced level of CO_2 in the blood. In NIRS, hypocapnia has been shown to result in an increased arterial volume fraction in the cerebral capillaries and a lower total hemoglobin signal. While changes in CO_2 levels have been shown to correlate with changes in total hemoglobin levels through this relationship, it assumes that the fraction of cerebral capillaries monitored by the NIRS are a reliable representation of the total brain volume [5].

While hypocapnia induces gradual signal variation over a number of respiratory cycles, signal changes on the time scale of the pulse and individual respiratory cycles are also visible in the NIRS signal [6]. Using a systems engineering approach to cerebral physiology, the effects of deep breathing

Manuscript received March 26, 2011. This work was supported in part by the U.S. Department of Education grant number P116Z080112.

P. M. Kennedy and C. M. Zarboarbock are with the Thayer School of Engineering at Dartmouth College, Hanover, NH 03755 USA.

B. A. Burke is with the Thayer School of Engineering at Dartmouth College, Hanover, NH 03755 USA as well as the Dartmouth Medical School, Hanover, NH 03755 USA.

S. G. Diamond is with the Thayer School of Engineering at Dartmouth College, Hanover, NH 03755 USA (phone: 603-646-1311; email Solomon.G.Diamond@dartmouth.edu).

on both a short and intermediate time scale were investigated using readily available instructional human physiology equipment to quantify the effect of deep breathing patterns on NIRS.

II. Methods

A. Experiment

The study protocol was approved by the Dartmouth College Committee for the Protection of Human Subjects and all subjects provided informed consent before participating. The study included five male subjects between the ages of 25 and 50.

Physiological signals were recorded using two BIOPAC transducer and acquisition systems (BIOPAC Systems, Inc. Goleta, CA). A 5L O_2/CO_2 gas analysis chamber (GASSYS2-EA) was connected to an airflow transducer (SS11LA) via a non-rebreathing T-valve so that only expired air was collected. Subjects breathed through a disposable mouthpiece (AFT2) connected to a bacterial filter (AFT1), affixed to the respiratory transducer. Finally, breathing was limited to the mouth by a disposable nose clip (AFT3). The respiratory transducer, O_2, and CO_2 outputs were connected to the BIOPAC MP36R analysis unit, which was connected to the BIOPAC PRO interface on a PC. Although the data is not presented herein, a simultaneous study required subjects to be connected to additional transducers, including a pulse plethysmogram (SS4LA), a stethoscope (SS30L) and blood pressure cuff (SS19L), and clip affixed ECG (SS2L). Finally, the NIRS system (TechEn CW6, TechEn, Inc. Milford, MA) consisted of 4 laser sources at each of the wavelengths 690, 785, 808, and 830 nm for a total of 16 lasers. The lasers were paired into eight optodes that were positioned on the forehead. Four detectors were configured below the source row of lasers. The NIRS apparatus was fit above the eyebrows and below the hairline. A total of 32 source-detector measurements were made on the forehead. Half of these measurements were combined into a left region of interest (ROI) and the remaining 16 into a right ROI. The source-detector separation ranged from 2cm to 4.5cm.

Before the experiment, the gas analyzer was equilibrated to room air using a small hand pump. The experimental protocol then consisted of four unique sections of breathing. First, subjects breathed normally through the respiratory transducer, disconnected from the gas analyzer, to practice breathing normally through the apparatus. For the second breathing section, the analyzer was connected and subjects breathed normally for 2 minutes, followed by a period of 2 minutes of deep breathing. For the deep breathing segments, subjects were instructed to inspire deeply at a comfortable frequency similar to that of normal breathing. Finally, subjects alternated between normal and deep breathing segments in one-minute increments for three cycles before ending with an extended period of 1.5 minutes of normal breathing.

B. Respiration data analysis

All collected data was categorized by subject numbers to protect anonymity and transferred to MATLAB (The MathWorks, Inc. Natick, MA) for post-processing. In the first series of data transformations, the output from the O_2 analyzer was converted from mole fraction per second to exhaled moles of O_2 per second. To do so, the mixing chamber of the gas analyzer was modeled as a simple first-order reactor:

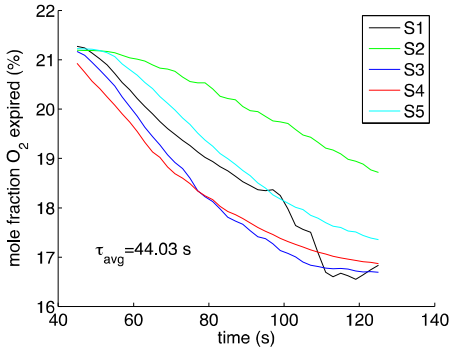

Fig. 1: Initial step input to instrument system

$$C_{in} = C_0 \exp\left(-(t-t_0)/\tau\right), \tag{4}$$

where C_{in} represents the concentration of O_2 input to the chamber and C_0 is the existing concentration at the end of the chamber. The exponential decay induced by the step response of breathing on the previously equilibrated chamber was then nonlinearly fit using the Nelder-Mead algorithm (via the *fminsearch* function in MATLAB).

Ideally, the instrument time constant τ would be measured for each subject. However, the time between connection to the gas analyzer and subsequent stimulation was too short and a few of the decaying exponentials did not resolve before the next stimulus was applied, making curve fitting inaccurate. Thus, τ_{avg} was calculated using the resolved exponential decays (subjects 1 & 3-5 in Fig. 1), although amplitude was individually calculated for each subject.

In order to elucidate the mole fraction of O_2 exhaled and remove the effect of the mixing chamber, the data was filtered using both the τ and C_0 from the non-linear curve fit. By using the Laplace domain analog of (4)

$$C(s) = \frac{C_0}{\tau_{avg} + s}, \tag{5}$$

the impulse response of the mixing chamber was simulated (using MATLAB's *impulse* function). Then, the original data was deconvolved with the impulse vector and smoothed with a moving block average with a 30-second window (for a multiple breath window).

In order to calculate the expired moles of O_2 per second, the time varying expired air volume needed to be calculated. The volume of exhaled air, given by the positive-valued airflow signal, was exported to a new array. Then, the array was smoothed with a moving block average with a window size of 5 seconds to remove the effect of individual breaths.

Next, the mole fraction of the corrected O_2 expired was converted to moles of expired air. The smoothed expired airflow per second, V_{exp}, was converted into moles of air per second with a modified form of the ideal gas law

$$n_{air} = \frac{P_{atm} V_{exp}}{RT}, \tag{6}$$

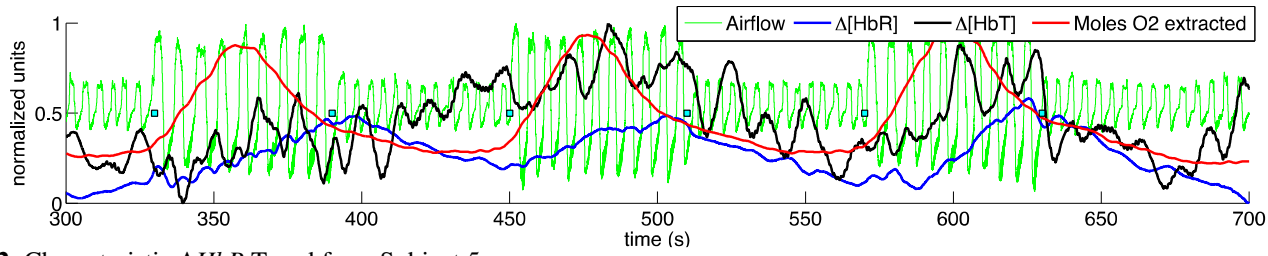

Fig. 2: Characteristic Δ*HbR* Trend from Subject 5

where n_{air} is the molar flow rate of expired O_2, R is the universal gas constant, and V_{exp} is the experimental expired flow data. The instrument corrected O_2 expired mole fraction was then multiplied by n_{air} to convert to moles of O_2 per second. Finally, the oxygen extracted by the subject was determined by solving the difference between the inspired and expired air. To do so, it was assumed that the percentage of oxygen in the room was constant over the experiment and the volume expired at body temperature is equivalent to the volume inspired at room temperature through Charles' Law.

C. NIRS data analysis

The NIRS data was sampled by the CW6 at 25 Hz and imported into MATLAB for data processing. First, the measured light intensity for each source-detector pair was converted to a time-varying change in optical density (Δ*OD*)

$$\Delta OD = -\log_{10}\left(\frac{I}{I_0}\right), \tag{7}$$

where the measured light intensity I is normalized by the initial intensity I_0. Hemoglobin concentration changes are related to optical density by the modified Beer-Lambert Law (MBLL) [7]

$$\Delta\mathbf{OD}(t) = \mathbf{F}\begin{bmatrix} \Delta HbO(t) \\ \Delta HbR(t) \end{bmatrix}, \tag{8}$$

where Δ**OD** is a column vector of optical density measurements for 16 source-detector measurements in a ROI at a given time point, and **F** is the MBLL forward model or design matrix with coefficients determined by the wavelength-dependent extinction coefficients of the hemoglobin species, source-detector separation, and differential path-length factor [8]. Equation 8 was solved for with an inverse noise-weighted Best Linear Unbiased Estimate (BLUE) [9] of the Δ*HbO*, Δ*HbR*. Measurement noise covariance **C** for the signals was estimated by computing variance in high-pass filtered Δ*OD* (obtained by subtracting a 0.12 second moving average).

$$\begin{bmatrix} \Delta\widehat{HbO}(t) \\ \Delta\widehat{HbR}(t) \end{bmatrix} = \left(\mathbf{F}^T\mathbf{C}^{-1}\mathbf{F}\right)^{-1}\mathbf{F}^T\Delta\mathbf{OD}(t), \tag{9}$$

This estimate yields output for both the left and right source-detector arrays for each of the calculated signals: Δ*HbO*, Δ*HbR*, and Δ*HbT* = Δ*HbO* + Δ*HbR*.

D. Cerebral Blood Flow

Two methods exist for calculating cerebral blood flow using NIRS. The "O_2 method" presented by Wyman is able to calculate numerical results with controlled O_2 inspired. The Δ*HbT* method, which if determined at two levels, can indicate the magnitude of a change in cerebral hemoglobin [10]. The second method assumes a constant proportionality between cerebral blood volume (CBV) and CBF. As only the physiological dynamics are of interest in the present study, the change in Δ*HbT* method was used in this analysis. This data is presented in Figs. 2 and 3 smoothed with a 5-second window to reduce the breath-to-breath effects.

E. Statistical Analysis

A peak detection algorithm in MATLAB was used to find the amplitudes of the NIRS Δ*HbT* signal from the 5-second window smoothed data. Then, the amplitude from periods of deep breathing versus periods of normal breathing were compared using a one-way analysis of variance (ANOVA).

III. Results

Figs. 2 and 3 present two different trends extracted from the deep breathing cycles. The first characteristic trend, observed in the data from subjects 1, 4, and 5 is shown for representative subject 5 in Fig. 2. The data indicates a correlation between rate of change of Δ*HbR* and extracted moles of O_2. The Δ*HbT* signal oscillates throughout the experiment but is not modulated by the stimulation cycle.

Conversely, a second characteristic trend, seen in subjects 2 and 3, is shown in Fig. 3 for representative subject 2. This trend shows little relation between extracted O_2 and Δ*HbR*. Instead, the Δ*HbT* signal shows large changes in oscillation amplitude during periods of deep breathing. Generally, this signal oscillates at lower levels during periods of deep breathing, although after three stimulation cycles the oscillation level appears to achieve a steady state value. Interestingly, the change in oscillation amplitude due to deep breathing stimulation between the subjects presented in Figs. 2 and 3 appears to be similar, although different trends in hemoglobin signal are observed.

The ANOVA results support these trends. The null hypothesis that the breathing methods are different was rejected at the 5% significance level for subjects 2 and 3 ($p=1.98\times10^{-8}$ and $p=0.0012$, respectively), while it could not be rejected for subjects 4 and 5. Subject 1 was not included because they followed a different breathing regimen.

IV. Discussion

The experiment simultaneously measured systemic and cerebral physiology to study the dynamic effect of deep breathing on the brain. Two dominant trends emerged from the deep breathing stimulation but to varying degrees in different subjects. In one subject, HbR increased during

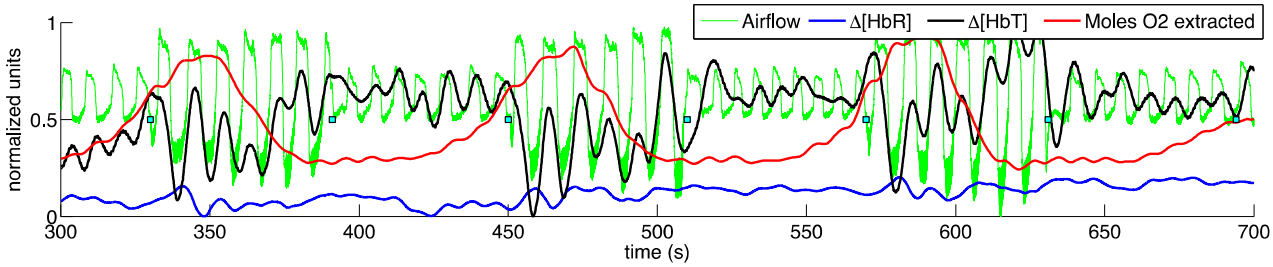

Fig. 3: Characteristic Δ*HbT* Trend from Subject 2

periods of deep breathing, and in others, the effect was synchronization between ventilation and HbT. One trend observed in both patients was increased oxygen extraction during the deep breathing segments. As this extraction subsides during continued deep breathing stimulus, this trend is likely the effect of O_2 saturation rather than physical work.

As shown in Fig. 2, changes in Δ*HbR* and extracted oxygen appear related. While the mechanism for this relationship is not revealed by the available measurements, one possible source is the effect of blood acidity on the regulation of CBF. CBF is highly responsive to changes in blood CO_2 levels (via the bicarbonate ion). With decreased acidity, cerebral blood vessels would constrict [3]. Assuming that the cerebral metabolic rate of oxygen is constant throughout the experiment, reduced CBF would result in an increase in Δ*HbR* as less CO_2 is removed over time. To a lesser extent, the decrease in CBF would lead to a corresponding decrease in the CBV, although this trend is not clear from the Δ*HbT* signal in Fig. 2.

As shown in Fig. 3, the same variation in breathing rate elicits a different response in subject 2. While it is assumed from the change in oxygen extraction that this subject enters a state of hypocapnia, little correlation exists between Δ*HbR* rate and the stimulation cycle. Additionally, the Δ*HbT* signal shows large signal oscillations between periods of deep and normal breathing. Therefore, a different physiological mechanism is likely responsible for the trend.

One such mechanism would be the increased hemoglobin saturation level in the blood during deep breathing. Because deep breathing increases the tidal volume of air inhaled and exhaled, the alveolar ventilation rate increases in periods of deep breathing, which is compensated for by an increase in the alveolar flow, Q_{gas}. This increase in flow could be the cause of the signal increase, since greater flow would correlate to a greater number of molecules present in the cerebral capillaries measured by the NIRS signal.

Because the Δ*HbR* signal shows little change throughout the experiment, it is assumed that unlike subject 5 from Fig. 2, CO_2 is removed equally well during different stimulation states. This suggests that the increased blood flow is strong enough to allow CO_2 to be effectively removed from the cerebral capillaries, even with vasoconstriction implied by the lower average Δ*HbT* signal during deep breathing. Combining the reduced CBV, vasoconstriction and strong flow, the oscillations in the Δ*HbT* can be explained by changes in pressure in the cerebral capillaries as a result of large amplitude flow variation.

V. Conclusion

Future studies should examine the difference between intercostal and diaphragmatic breathing, which may explain the variation between the example subjects. Intercostal breathing utilizes less of the useful lung volume so the inspired partial pressure of oxygen at the alveoli is reduced. Intercostal breathing also places the chest under additional pressure that may induce the amplitude response shown in the deep breathing section of this experiment for the subject presented in Fig. 3. Thus, higher pressures would force the Δ*HbT* signal to larger amplitudes during periods of deep breathing. Conversely, diaphragmatic breathing utilizes more of the available oxygen, likely resulting in a larger shift in the hemoglobin-dissociation curve leading to increased vasoconstriction, mirrored in the Δ*HbR* signal.

Although future studies are required to further investigate differences in breathing technique and corresponding hemoglobin changes, this study provides a foundation for future investigations into breathing technique and reaffirms the feasibility of the simple experimental method. Further, the difference between these breathing techniques may be a clinically useful metric, as deep breathing is an often utilized therapy for a variety of conditions and understanding the effects of each breathing method on cerebral hemoglobin dynamics could allow for more useful treatment.

References

[1] R. P. Brown and P. L. Gerbarg, "Yoga breathing, meditation, and longevity," *Ann. NY Acad. Sci.*, vol. 1172, pp. 54-62, 2009.

[2] J. P. Keener and J. Sneyd. *Mathematical Physiology*. New York: Springer, 2009.

[3] A. C. Guyton and J. E. Hall. *Textbook of Medical Physiology*. 11th ed. Philadelphia: Elsevier Saunders, 2006.

[4] A. P. Gibson, J. C. Hebden, and S. R. Arridge, "Recent Advances in Diffuse Optical Imaging," *Phys. Med. Biol.*, vol. 50, pp. R1-43, 2005.

[5] P. Rasmussen *et al*, "Capillary-oxygenation-level-dependent near-infrared spectrometry in frontal lobe of humans," *J Cereb. Blood Flow Metab.*, vol. 27, no. 5, pp. 1082-1093, 2007.

[6] C. E. Elwell, *et al.*, "Quantification of adult cerebral hemodynamics by near-infrared spectroscopy," *J Appl. Physiol.*, vol. 77, no. 6, pp. 2753-2760, 1994.

[7] M. Cope *et al*., "Methods of quantitating cerebral near infrared spectroscopy data," *Adv. Exp. Med.* Biol, vol. 222, pp. 183-189, 1988.

[8] D. T. Delpy *et al.*,"Estimation of optical pathlength through tissue from direct time of flight measurement," *Phys. Med. Biol.*, vol. 33, pp. 1433–1442, 1988.

[9] M. S. Kay. *Fundamentals of Statistical Signal Processing. Estimation Theory.* Prentice-Hall, 1993.

[10] M. Firbank *et al*., "Experimental and Theoretical Comparison of NIR Spectroscopy Measurements of Cerebral Hemoglobin Changes," *J Appl. Physiol.*, vol. 85, no. 5, pp. 1915-1921, 1998.